Published by Avanti Publishers

International Journal of Petroleum Technology

ISSN (online): 2409-787X

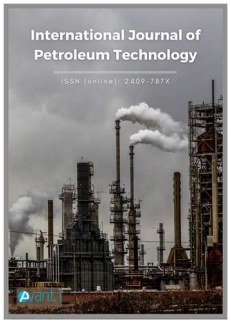

Fabrication and Characterization of Thin-Film SOFC Supported by Microchannel-Structured Zirconia Substrate for Direct Methane Operation

Myongjin Lee, Yun Gan, Chunyang Yang, Chunlei Ren and Xingjian Xue*

Department of Mechanical Engineering, University of South Carolina, Columbia, SC 29208, USA

ARTICLE INFO

Article Type: Research Article

Keywords:
Stability
Ni-ZrSDC Anode
Hydrocarbon Fuels
Microtubular SOFC
Microchanneled Inert Support

Timeline:
Received: August 20, 2021
Accepted: September 20, 2021
Published: October 12, 2021

Citation: Lee M, Gan Y, Yang C, Ren C, Xue X. Fabrication and Characterization of Thin-Film SOFC Supported by Microchannel-Structured Zirconia Substrate for Direct Methane Operation. Int J Petrol Technol. 2021; 8: 80-92.

DOI: https://doi.org/10.15377/2409-787X.2021.08.6

ABSTRACT

Ni-cermet anode demonstrates excellent catalytic activity and electrical conductivity but suffers from carbon deposition issues. To utilize Ni-cermet anode while preventing carbon deposition, a synergic strategy is employed to design anode electrodes. In particular, Zr is incorporated into $Ce_{0.8}Sm_{0.2}O_{2-\delta}$ lattice to tailor oxygen storage and catalytic properties of Ni-$Ce_{0.8-x}Sm_{0.2}Zr_xO_{2-\delta}$ anode for improving electrochemical oxidization of various fuel species. An inert thick YSZ microtubular substrate with radially well-aligned microchannels open at the inner surface supports multi-thin functional layers of solid oxide cell, i.e., Ni current collector, Ni-$Ce_{0.8-x}Sm_{0.2}Zr_xO_{2-\delta}$ anode, YSZ/SDC electrolyte, and LSCF cathode. The thick YSZ substrate inhibits the ratio of fuel to product gases in the thin anode functional layer, which favors the prevention of carbon build up in the thin anode layer when synergistically combined with Ni-$Ce_{0.8-x}Sm_{0.2}Zr_xO_{2-\delta}$ anode material. The microchannels embedded in the YSZ substrate can also avoid too much fuel dilution in the anode functional layer. The cell is fabricated and tested with both hydrogen and methane as the fuel. A short-term test is conducted with methane as fuel, and good stability is obtained. The fundamental mechanisms for the prevention of carbon build up in the anode functional layer are also discussed.

*Corresponding Author
Emails: xue@cec.sc.edu
Tel: 803-576-5598

1. Introduction

Solid oxide fuel cell (SOFC) is an energy conversion device that converts chemical energy in fuels into electrical energy very efficiently and is environmentally friendly. SOFCs are fuel flexible that can use not only hydrogen but hydrocarbon fuels and even carbon [1-4]. Direct hydrocarbon-fueled SOFCs may provide advantages of eliminating external reforming components for SOFC systems and using the existing infrastructures for the production, storage, and delivery of hydrocarbon fuels. These would improve system efficiency, reduce system cost, and facilitate practical applications of SOFC technologies. The state-of-the-art anode material is Ni-cermet, a composite of Ni and electrolyte material. The Ni phase is an electronic conductor and catalyst, while the electrolyte phase is an ionic conductor. The catalytic activity of Ni enables the reforming of hydrocarbon fuels for producing syngas, a mixture of H_2 and CO, through catalytic oxidation, such as steam reforming and CO_2 reforming as well as water-gas shift reaction. However, the high catalytic activity of Ni can also lead to the direct cracking of hydrocarbon compounds at high temperatures and CO hydrogenation as well as Boudouard reaction, causing carbon deposition in the anode. The carbon deposition, in turn, will deactivate active reaction sites, restrict gas flow, and damage microstructures, overall leading to severe degradations in anode performance and long-term stability [5-9]. Therefore, the carbon deposition issue in Ni-cermet anode electrode of hydrocarbon-fueled SOFCs has been a major barrier towards practical applications.

Significant efforts have been made to modify Ni-cermet anodes to improve their properties for carbon deposition resistance. These include surface modification and alloying of Ni-cermet with carbon-resistant metals and oxides, such as Cu, Sn, Ag, Ru, W, CeO_2, and their derivatives [10-19]. Despite these modifications, it is generally realized that the carbon deposition issue is inevitable for Ni-based anodes due to the Ni-catalytic cracking of hydrocarbon fuels, especially in large-scale applications. Attempts have been made to develop Ni-free anode materials to circumvent the use of Ni-based anode. These typically include a class of perovskite- and layered perovskite-type of mixed ionic and electronic conducting oxides, such as $La_{0.75}Sr_{0.25}Cr_{0.5}Mn_{0.5}O_3$, $La_{1-x}Sr_xTiO_3$, $Sr_2Mg_{1-x}Mn_xMoO_{6-\delta}$, $PrBaMn_2O_{5+\delta}$, and their derivatives [20-24]. Despite the fact that such materials demonstrated good properties as anodes for carbon deposition resistance, the power densities of corresponding SOFCs are usually much lower than Ni-cermet counterparts.

Further, complete conversion from hydrocarbon to syngas is hardly to achieve with such Ni-free anode materials. In this context, Ni-cermet is still a preferred anode material due to its high electronic conductivity and (electro)catalytic properties [25]. Another strategy to mitigate the carbon deposition issue is co-feeding a considerable amount of water with hydrocarbon fuels so that the oxygen to carbon ratio is maintained at a sufficiently high level in anode electrode. As a result, complete internal reforming of hydrocarbon fuels can be obtained. Meanwhile, it can also prevent Ni from being oxidized. However, too much water supply will dilute fuels in the anode, which in turn decreases open-circuit voltage and deteriorate the electrochemical performance of SOFCs. In this respect, precise control of operating temperature and oxygen to carbon ratio in the anode electrode may need much less water feeding. Nevertheless, the operation under precisely controlled thermodynamic conditions is possible but not practically feasible [26].

Recently, the concept of a diffusion barrier layer has been employed to increase diffusion resistance of hydrocarbon fuels into the anode functional layer and product gases (i.e., H_2O, CO_2) out of the anode functional layer. As a consequence, the concentration ratio of product gases to hydrocarbon fuel in the anode functional layer will be high enough to suppress carbon build up in the anode functional layer [27-29]. On the one hand, the diffusion barrier layer increases fuel/gas diffusion resistance and concentration polarization loss of the anode; on the other hand, the high concentration ratio of product gases to hydrocarbon fuel will dilute fuels in the anode functional layer. Both of the effects will deteriorate the electrochemical performance of SOFCs. Therefore, a trade off is needed between carbon deposition suppression and good electrochemical performance when the diffusion barrier layer is employed for anode electrodes. One strategy for such a trade off could be obtained through a synergistic combination of a diffusion barrier layer and suitable Ni-cermet anode material. The diffusion barrier layer is used to tune carbon/oxygen ratios without diluting fuels too much in the anode functional layer. This requires that the porous microstructure of barrier layers enable facile fuel/gas diffusions. The Ni-cermet anode material should possess sound oxygen storage and catalytic properties, enabling full electrochemical oxidization

of fuel species. As a result, H_2O and CO_2 produced by full oxidization of fuel would suppress carbon build up through backward Boudouard reaction and hydrogenation.

Cerium oxide exhibits the property of releasing and incorporating oxygen [30-31]. When aliovalent ions (divalent or tetravalent cations) are doped into ceria lattice, it may create oxygen vacancies by charge compensation mechanism, further improving oxygen storage capacity and catalytic property of ceria [32-34]. In this research, Zr and Sm were co-doped into ceria lattice and NiO – $Ce_{0.8-x}Sm_{0.2}Zr_xO_{2-\delta}$ (NiO:$Ce_{0.8-x}Sm_{0.2}Zr_xO_{2-\delta}$ = 50%:50% in weight; x=0, 0.05, 0.10, 0.15, and 0.20, or simply denoted as NiO-ZrxSDC) as anode materials were systematically studied. The Zr doping level that minimizes polarization resistance of NiO-ZrxSDC anode was identified. A microtubular YSZ inert substrate was fabricated using an in-house built spinning extrusion system, featuring radially well-aligned microchannels open at the inner surface. Built upon the microtubular YSZ substrate and the identified NiO-Zr0.1SDC anode material, inert YSZ substrate supported cell of YSZ substrate/NiO/NiO-Zr0.1SDC/YSZ/$Ce_{0.8}Sm_{0.2}O_{1.9}$/$La_{0.6}Sr_{0.4}Co_{0.2}Fe_{0.8}O_{3-\delta}$ was fabricated through dip-coating and sintering process alternatively. The combination of such a cell design with NiO-Zr0.1SDC anode material is expected to suppress carbon deposition in the anode functional layer, thereby achieving stable electrochemical performance with hydrocarbon fuels.

2. Experimental

2.1. Material Synthesis

All the chemicals used in the experiments were purchased from Alfa Aesar and used as-purchased unless otherwise specified. The anode powders of 50% NiO – 50% $Ce_{0.8-x}Sm_{0.2}Zr_xO_{1.9}$ (NiO-ZrxSDC) in weight were synthesized by a urea combustion method in one pot. Particularly, stoichiometric amounts of $NiO(NO_3)_2{\cdot}6H_2O$ (98.0% purity), $Ce(NO_3)_3{\cdot}6H_2O$ (99.5% purity), $Sm(NO_3)_3{\cdot}6H_2O$ (99.9% purity), Zirconyl nitrate solution (99.0% purity), and urea ($CO(NH_2)_2$) (99.0-100.5% purity) were dissolved into deionized water to form a solution. The solution was magnetically stirred for 3hrs, followed by heating on a hot plate until self-ignited. After self-sustaining combustion, ash-like material was obtained. The obtained ash was subsequently ground for 24hrs in an ethanol medium using a ball milling process with zirconia balls. After drying, the ash was calcinated at 1000°C in the air for 2hrs to form NiO-ZrxSDC phases. $La_{0.6}Sr_{0.4}Co_{0.2}Fe_{0.8}O_{3-\delta}$ (LSCF) powders were synthesized by a glycine nitrate process. Briefly, stoichiometric amounts of $La(NO_3)_3{\cdot}6H_2O$ (99.9% purity), $Sr(NO_3)_2$ (99.0% purity), $Co(NO_3)_3{\cdot}6H_2O$ (97.7% purity), $Fe(NO_3)_3{\cdot}9H_2O$ (98.0-101.0% purity) and glycine (99.5% purity) were dissolved into deionized water to form a solution. The solution was magnetically stirred for 3hrs followed by heating on a hot plate until combustion, resulting in ash-like material. The obtained ash-like material was subsequently ground for 24hrs in ethanol medium using a ball milling process with zirconia balls. After drying, the ash was calcinated at 700°C in the air for 2hrs to form the LSCF phase.

2.2. Symmetric Button Cell Preparation

The SDC powders (Fuel Cell Materials, USA) with the binder of 2% polyvinyl butyral in weight were mixed and ground in ethanol. After drying, the mixture of powder and binder was iso-statically cold-pressed at 600MPa to form an electrolyte substrate, resulting in a diameter of ~ 10mm and a thickness of ~1mm. The green electrolyte substrate was then sintered at 1450°C in the air for 6hrs to form a dense SDC electrolyte. The surface of sintered SDC electrolyte substrate was mechanically polished using sand-papers and subsequently washed by anhydrous ethanol in an ultrasonic cleaner. The resulting thickness of SDC electrolyte substrates was about 400μm. 5% ethyl-cellulose (TCI, Japan) in weight was mixed with 95% α-terpineol (TCI, Japan) in weight to form an organic solution. The synthesized fine powders (NiO-ZrxSDC, 66.67% in weight) were then mixed with the organic solution (33.33% in weight) to form electrode inks. The electrode inks were screen-printed onto either side of the dense SDC electrolyte substrate. After drying and aging, the electrode-electrolyte assembly was sintered at 1250°C in the air for 2hrs to form symmetrical cell NiO-ZrxSDC | SDC | NiO-ZrxSDC. Silver wire was attached to either side of the symmetrical cells using silver paste (Heraeus 2807) as a current collector and external wires for further electrochemical measurement.

2.3. Single Microtubular Cell Fabrication

Microtubular YSZ inert substrate was first prepared. Briefly, polyethersulfone (PESf, Veradel 3000P, Solvay Specialty Polymers, USA; 3.5% in weight) and polyvinylpyrrolidone (PVP, K30, CP, Sinopharm Chemical Reagent Co., China; 0.5% in weight) were dissolved in N-methyl-2-pyrrolidone (NMP, HPLC grade, Sigma Aldrich, USA; 21% in weight) and ball-milled for 2hrs to form an organic mixture. Commercial YSZ powder (Tape grade, Fuel Cell Material, USA; 75.0% in weight) was added into the organic mixture and ball-milled for 48hrs to form a homogeneous extrusion slurry. The as-prepared slurry was de-aired for 10 min and then loaded into an in-house build spinneret extrusion system to obtain green microtubular substrate. The extrusion system and related extrusion process were detailed elsewhere [35-37]. The green substrate was sintered at 1100^{o}C in the air for 3hrs to achieve sufficient mechanical strength for subsequent functional layer coatings of NiO, NiO-Zr0.1SDC, YSZ, SDC, and LSCF sequentially. In particular, 0.4% ethyl cellulose and 99.6% ethanol in weight were mixed together to form an organic solution. 16.0% NiO (Fuel cell materials, USA) and 1.8% potato starch (J.T. Baker, USA) powders in weight were then mixed with the organic solvent to form a NiO slurry. The sintered YSZ microtubular substrates were sealed at both ends using PTFE films and vertically immersed into the prepared NiO slurry for 30 seconds. After drying in the air for 12hrs, the coated samples were calcinated at 600^{o}C in the air for 30min to burn out organics and bind the NiO layer onto the YSZ substrate. The preparation and coating of NiO-Zr0.1SDC slurry were similar to those of the NiO layer but calcined at 900^{o}C in air for 1hr. For YSZ electrolyte fabrication, 30% B73210 organic binder in weight (Ferro Electronics Materials, USA), 40% α-terpineol in weight, and 30% ethanol in weight were first mixed to form an organic slurry. 17% YSZ powders (Fuel cell materials, USA) in weight were then mixed with the organic slurry to form a YSZ slurry. The YSZ slurry was then dip-coated onto the NiO-Zr0.1SDC layer, followed by dip-coating a SDC layer in a similar way. After drying, the coated samples were sintered at 1400^{o}C in the air for 4hrs to form half-cells. Finally, the LSCF cathode layer was fabricated. Specifically, an organic slurry was first prepared by mixing 63.0% 2-butanone, 31.0% ethanol, 0.5% triethanolamine, 1.0% dibutyl phthalate, 1.0% polyethylene glycol 300 (ACROS, USA), and 3.5% butvar B-98 (Spectrum, USA) in weight. 10.0% LSCF powders were then mixed with the prepared organic slurry to form a LSCF cathode slurry. The LSCF cathode slurry was then dip-coated onto the half-cells. After drying, the coated samples were sintered at 950 ^{o}C in the air for 2hrs to form a single microtubular cell of YSZ substrate/NiO/NiO-ZSDC/YSZ/SDC/LSCF. The resulting cathode area was about 0.3 cm^{2}. The silver paste was painted onto the cathode as a current collector. Silver wire was wound around the cathode and at either end of the anode substrate to serve as a current collector and external circuit.

2.4. Characterization and Electrochemical Measurements

The phase purity of the prepared powder materials was characterized and identified using the X-ray diffraction technique (XRD, D/MAX-3C) with Cu Kα radiation (λ=1.5406 Å) at room temperature with a scanning rate of 5^{o} min^{-1} in the range of 20^{o} ≤ 2θ ≤ 80^{o}. Microstructures of prepared samples and cells were characterized using scanning electron microscopy (SEM, Zeiss Ultra Plus FESEM, Germany). Microstructures and element distributions of prepared microtubular cells were also examined using SEM in combination with Energy-dispersive X-ray spectroscopy (EDS, Oxford Instruments detector).

The symmetrical cell prepared above was sealed in an alumina test chamber. A high-temperature tube furnace controlled the temperature of the chamber. The temperature of the furnace was increased from room temperature to 800^{o}C at a rate of 2^{o}C min^{-1} while nitrogen with the flow rate of 30 ml min^{-1} was supplied into the alumina chamber. Once the furnace temperature reached 800^{o}C, the supplied gas was switched from nitrogen to humidified hydrogen (~3% H_2O, 30 cm^{3} min^{-1}). Under this condition, the experiment lasted for 3hrs, allowing the completion of NiO reduction to Ni in the electrodes. Electrochemical impedance spectra (EIS) of the symmetric cell were then measured using the Solartron1260/1297 electrochemical workstation. The EIS measurement was obtained from 800 to 600^{o}C with a voltage perturbation of 10mV over the frequency range from 0.01Hz to 1MHz under open circuit voltage conditions.

The fabricated microtubular cell was electrochemically tested from 600 to 800^{o}C. Both humidified hydrogen and methane were used as fuel, while ambient air was used as an oxidant. The surface of the cathode and anode electrode was coated with silver paste and encircled with silver wires as the current collectors. Ceramic paste (Aremco products, inc. USA) was used to seal and attach two alumina tubes to either end of the YSZ substrate of

the cell. The procedure is detailed in the paper published elsewhere [35]. The temperature of the cell was controlled by a tube furnace (MTI, USA). Nitrogen gas was first supplied into the anode of the cell at room temperature. The cell was then heated up from room temperature to 800°C at the rate of 2°C min^{-1}. Once the cell temperature reached 800°C, the gas supplied to the anode was switched from nitrogen to humidified hydrogen (~3% H_2O). The flow rate of hydrogen was controlled at 30 cm^3 min^{-1} using a precision flowmeter (APEX). The reduction of NiO current collector layer and NiO-Zr0.1SDC anode functional layer under this condition lasted for 3hrs before electrochemical testing. The voltage-current (V-I) curves and EIS were measured using a Solartron1260/1287 electrochemical workstation from 800 to 600°C. The EIS measurements were performed with a voltage perturbation of 10 mV over the frequency range from 0.01Hz to 1MHz under open-circuit voltage conditions. Similarly, V-I curves and EIS of the cell were measured using methane as fuel with the flow rate of 30 cm^3 min^{-1} in the temperature range of 600 – 800°C. A short-term stability test was also carried out with methane as fuel at an operating temperature of 700°C. The voltage of 0.7V was applied to the cell while the time history of current cell density was recorded.

3. Results and Discussion

3.1. Materials Characterization

Fig. (**1a**) shows the XRD patterns of the synthesized NiO-$Ce_{0.8-x}Sm_{0.2}Zr_xO_{2-\delta}$ (NiO-ZrxSDC, x= 0.05, 0.10, 0.15, and 0.20) powders. All characteristic diffraction peaks correspond to the NiO and ZrxSDC phases. No other phases could be detected, implying that Zr was totally dissolved into the SDC lattice. The XRD patterns further indicate very good chemical compatibility between NiO and ZrxSDC phases. Fig. (**1b**) shows the XRD patterns of the powders in the 2θ range of 54-58°. It can be seen that the peak was shifted to the higher angles with increasing Zr dopant contents from 0.05% mol to 0.20% mol, indicating the decrease of lattice volume. Since the atomic radius of Zr^{4+} (80Å) is smaller than that of Ce^{4+} (90Å), the Zr doping leads to the decreased lattice parameter.

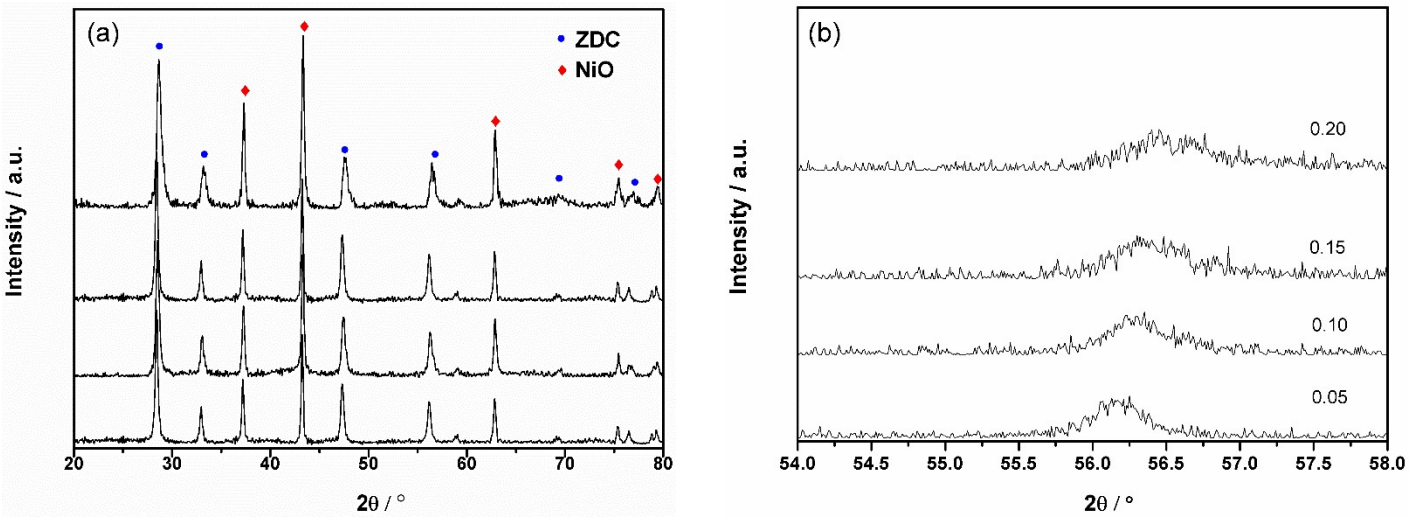

Figure 1: (a) XRD patterns of synthesized NiO-ZrxSDC powders in the 2θ range of 20-80°. (b) XRD patterns of the powders in the 2θ range of 54-58°.

Fig. (**2**) shows SEM images of the synthesized NiO-ZrxSDC powders. The powders consisted of fine and homogeneous particles with certain agglomerations. The average size of agglomerations is about 545nm. It seems that the agglomerations become weaker beyond the Zr doping level of 0.05.

3.2. Symmetry Cells

Fig. (**3**) shows the polarization resistances (R_p) values of the symmetrical cells Ni-ZrxSDC|SDC|Ni-ZrxSDC (x = 0, 0.05, 0.10, 0.15, and 0.20) measured in humidified hydrogen at the temperatures of 600 – 800°C. The R_p values of

different Zr doping levels at different temperatures were obtained from the equivalent circuit technique fitting from the EIS curves. The obtained $R_p$values were then corrected by the electrode area and divided by two due to the symmetrical configuration of the cell. It can be seen that the polarization resistance tended to decrease with increasing Zr doping level in the range of 0 to 0.1% mol at every operating temperature. Beyond 0.1% mol, the polarization resistance increased with increasing Zr dopant. The Ni-Zr0.1SDC electrode obtained the minimum polarization resistance among different Zr doping levels. In what follows, NiO-Zr0.1SDC will be used as anode material to fabricate microtubular YSZ inert substrate-supported single cell for electrochemical performance study.

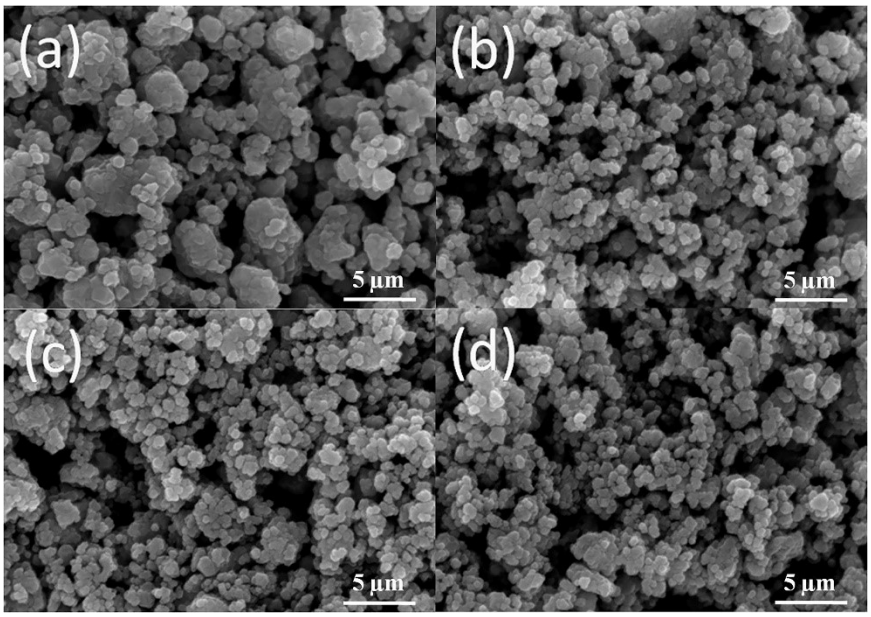

Figure 2: SEM images of the synthesized NiO-ZrxSDC powders. (a) x=0.05, (b) x= 0.10, (c) x= 0.15 and (d) x= 0.20.

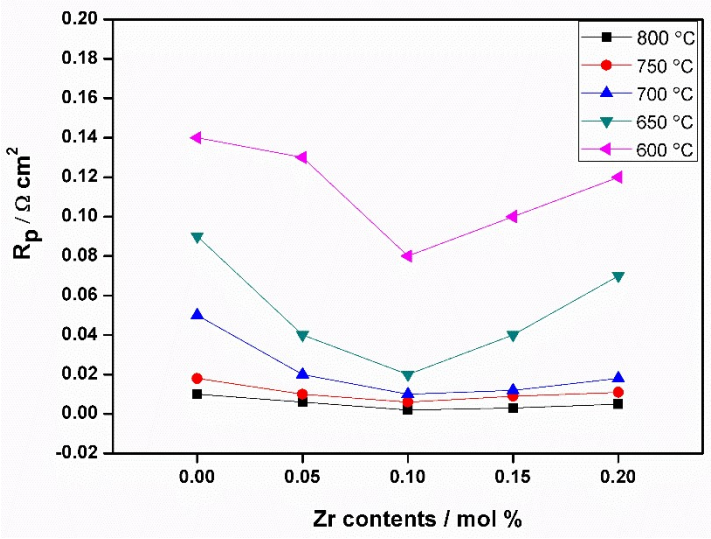

Figure 3: Polarization resistance (R_p) of the Ni-ZrxSDC electrode symmetry cell.

3.3. Single-Cell Performances

Fig. (**4**) shows a cross-sectional SEM image of the fabricated microtubular cell YSZ substrate/NiO/NiO-Zr0.1SDC/YSZ/SDC/LSCF. It can be seen that radially well-aligned microchannels were embedded in the thick YSZ substrate, which is open at the inner surface (Fig. **4a**). Multiple functional layers can also be observed on the thick YSZ substrate, including ~3µm NiO current collector layer, ~4µm NiO-Zr0.1SDC anode functional layer, ~10µm YSZ

electrolyte layer, ~5μm SDC buffer layer, and ~10μm LSCF cathode layer (Fig. **4b**). Intimate adhesions were obtained between different layers. The YSZ electrolyte layer is very dense. The SDC layer contains closed pores but is good enough as a buffer layer to separate the YSZ electrolyte layer from the LSCF cathode layer, which allows avoiding chemical reactions between YSZ and LSCF at elevated temperatures. The NiO layers and NiO-Zr0.1SDC exhibited porous microstructure features, and the porosity would be further improved in these two layers after NiO is reduced to Ni.

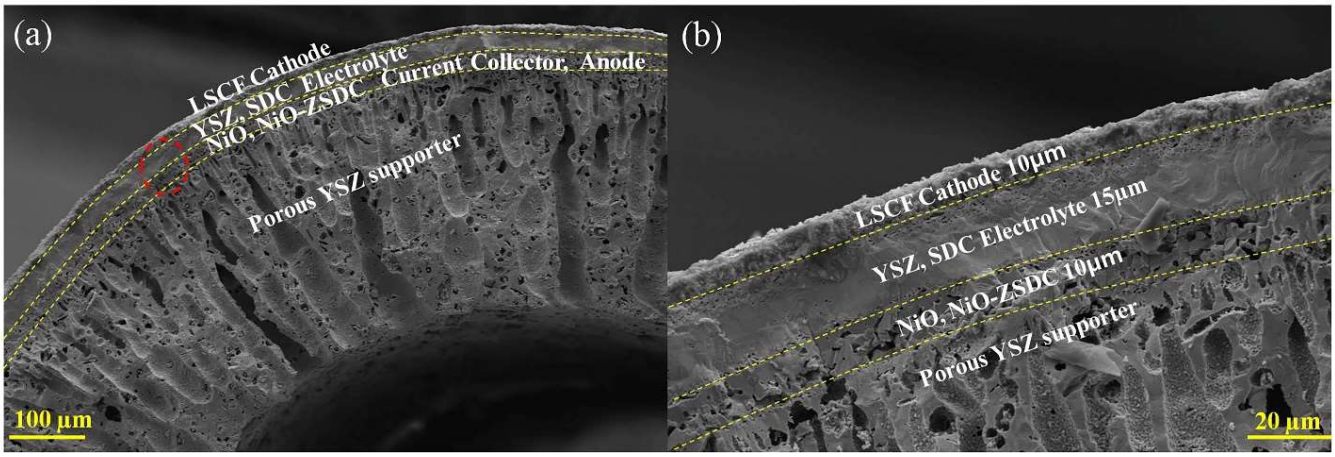

Figure 4: (a) SEM cross-sectional image of as-prepared porous YSZ supported single cell. (b) Enlarged SEM image of local area marked with the red circle in (a).

To examine the quality of the fabricated cell in a comprehensive manner, a benchmark test was first carried out. Before the test, the NiO current collector and NiO-Zr0.1SDC anode functional layer were first reduced. In particular, nitrogen with the flow rate of 30 cm^3 min^{-1} was supplied to the anode side while the cell was heated up by a tube furnace. When the cell temperature reached 800°C, the supplied nitrogen was switched to humidified hydrogen with a flow rate of 30 cm^3 min^{-1}. The experiment under this condition was lasted for 3 hrs, allowing for the completion of NiO reduction. The electrochemical performance of the cell was then measured in the temperature range of 800 – 600°C, with the cathode electrode being exposed to ambient air. Fig. (**5a**) shows the corresponding voltage-current (V-I) curves and power density (P-I) curves. The OCVs of 1.01 to 0.94 V were obtained at the temperature range of 600 – 800°C. These values are close to the theoretical Nernst potentials (e.g., ~1.10V) when YSZ is employed as electrolyte material, indicating that the YSZ electrolyte is dense and the rest of the cell components functioned well. The results further imply that the process for cell fabrication is reliable. The peak power density of the cell reached about 204, 272, 385, 500, and 602 mW cm^{-2} at 600, 650, 700, 750, and 800°C, respectively. The EIS curves of the cell measured at OCV conditions are shown in Fig. (**5b**). Using equivalent circuit and curve-fitting technique, the ohmic resistance (R_{ohm}) and polarization resistance (R_p) of the cell were obtained from EIS curves and listed in Table **1**. As one can see that with increasing the operating temperature from 600 to 800°C, the cell R_{ohm} decreased from 0.93 to 0.25 Ω cm^2 while the cell R_p decreased from 1.12 to 0.23 Ω cm^2, respectively. The R_{ohm} is contributed by electrolyte and the skeleton of porous anode and cathode electrode as well as associated current collectors. The increasing temperature would directly reduce ohmic resistances of YSZ

Table 1: Open circuit voltage (OCV), ohmic resistance (R_{ohm}), polarization resistance (R_p), maximum power density (MPD) of the single cell in hydrogen at different temperatures.

Temperature / ℃	800	750	700	650	600
OCV / V	0.94	0.96	0.988	1.00	1.01
MPD / $mWcm^{-2}$	602	500	385	272	204
R_{ohm} / Ω cm^2	0.25	0.46	0.71	0.82	0.93
R_p / Ω cm^2	0.23	0.45	0.67	0.94	1.12

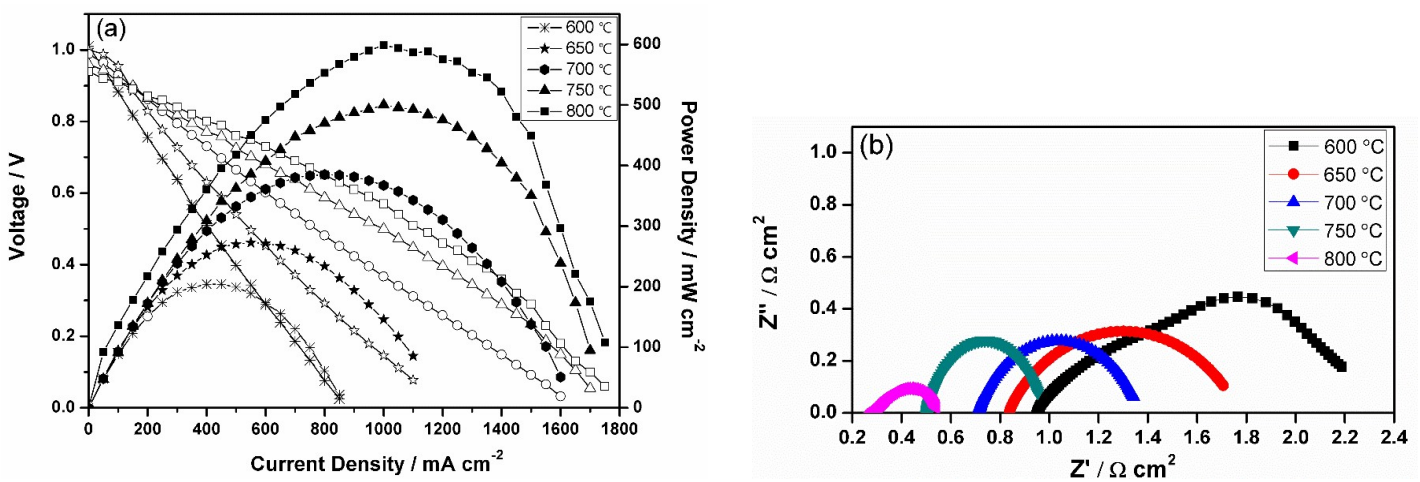

Figure 5: (a) V-I curves and power density curves of the single cell in hydrogen. (b) EIS curves of the single cell in hydrogen under open circuit voltage conditions.

electrolyte and Ni-Zr0.1SDC anode as well as LSCF cathode skeletons; therefore, the cell R_{ohm} decreased. Similarly, higher temperatures would enhance the electrochemical kinetic properties of both anode and cathode electrodes, including surface exchange coefficients and bulk diffusivities. Accordingly, the cell R_p decreased. Overall, the benchmark test results indicate that the cell obtained reasonably good electrochemical performance, confirming that the cell fabrication process is reliable. The electrochemical performance of the fabricated cell fueled with methane is then tested. The effectiveness of a synergistic combination of Ni-Zr0.1SDC anode material and cell architecture for suppression of carbon deposition is further examined.

Shown in Fig. (**6a**) are V-I curves and P-I curves of the cell directly fueled with methane in the temperature range of 600 – 800°C. The cell obtained OCVs of 1.02, 1.01, 1.00, 0.98, and 0.967V and peak power densities of 173, 259, 327, 384, and 456 mW·cm^{-2} at the temperatures of 600, 650, 700, 750, and 800°C, respectively. Fig. (**6b**) shows the EIS curves of the cell under open-circuit voltage conditions. Using equivalent circuit and curve-fitting technique, the cell ohmic resistance (R_{ohm}) and polarization resistance (R_p) were obtained from the measured EIS curves. The results are summarized in Table **2**. In particular, the ohmic resistance of 0.45, 0.52, 1.05, 1.57, and 1.98 Ω cm^2 and the polarization resistance of 0.47, 0.51, 0.89, 1.23, and 1.43 Ωcm^2 were obtained at the temperatures of 600, 650, 700, 750, and 800°C, respectively.

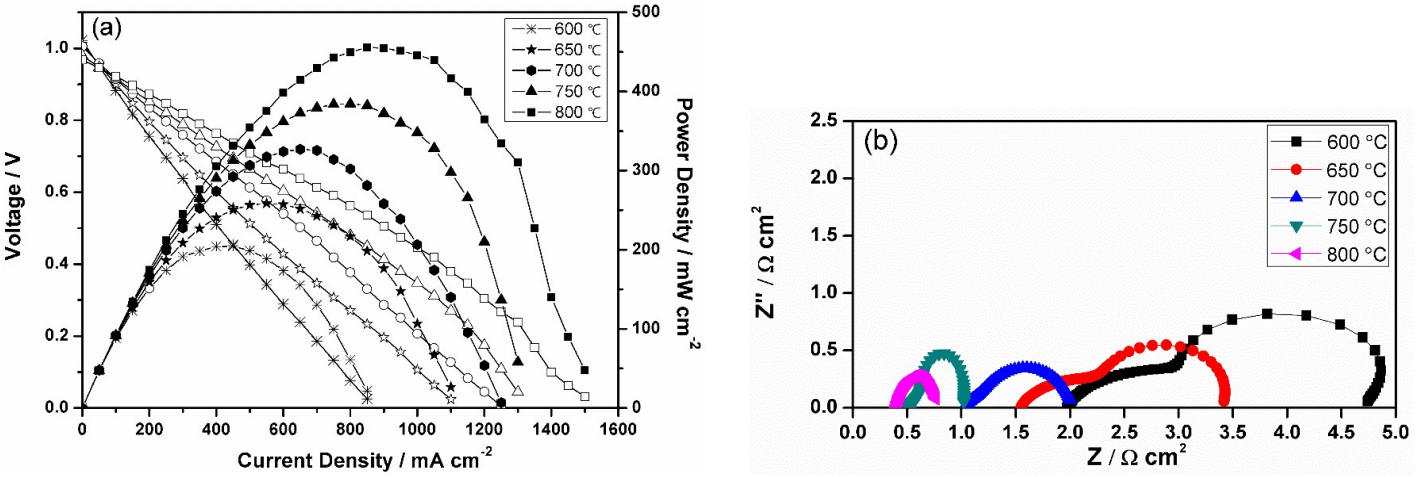

Figure 6: (a) V-I curves and power density curves of the single cell in methane. (b) EIS curves of the single cell in methane under open circuit voltage conditions.

To examine the stability of the cell directly fueled with methane, a short-term durability test was carried out. The temperature of the cell was controlled at 700°C. The voltage of 0.7V was applied to the cell while the current

of the cell was monitored. Under these conditions, the experiment was run for about 26hrs. The history of current cell density is shown in Fig. (**7**). It is obvious to see that the current density of the cell was very stable, performance degradations could not be observed. It is noteworthy that methane-fueled YSZ inert substrate-supported SOFC has been studied in the open literature [38], where Ni-SDC was used as anode functional layer material, and the porosity of YSZ substrate was randomly distributed without any radially well-aligned microchannels. Nevertheless, the corresponding cell showed a voltage loss of 9% during short-term stability of 13 hrs at 700°C in methane. Comparing our results mentioned above with those in [38], it seems to indicate that the combination of Zr doped SDC anode material and YSZ inert substrate embedded with radially well-aligned microchannels is able to effectively improve the performance stability of the cell directly fueled with methane. After the short-term durability test, the cell was further characterized. Shown in Fig. (**8a**) is the cross-sectional SEM image of the post-test microtubular cell ranging from part of the YSZ substrate to part of the dense YSZ electrolyte.

Table 2: Open circuit voltage (OCV), ohmic resistance (R_{ohm}), polarization resistance (R_p), maximum power density (MPD) of the single cell in methane at different temperatures.

Temperature / ℃	800	750	700	650	600
OCV / V	0.967	0.98	1.00	1.01	1.02
MPD / $mWcm^{-2}$	456	384	327	259	173
R_{ohm} / Ω cm^2	0.45	0.52	1.05	1.57	1.98
R_p / Ω cm^2	0.47	0.51	0.89	1.23	1.43

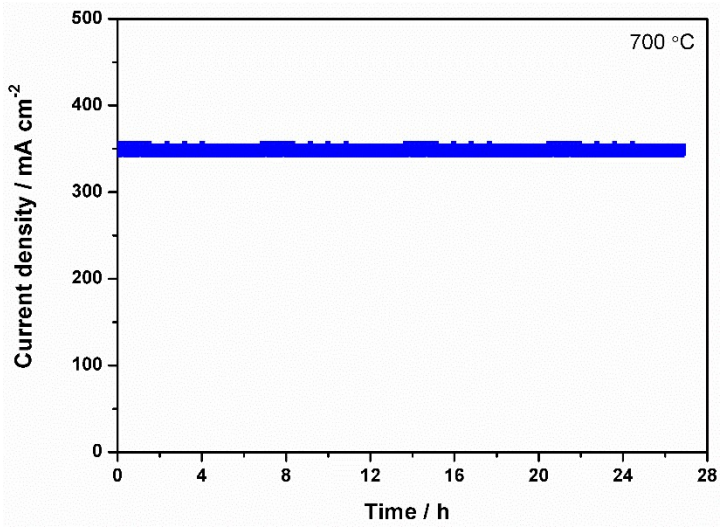

Figure 7: Short-term performance stability of the single cell in methane fuel at 0.7 V and 700°C.

The radially well-aligned microchannels in the YSZ substrate still can be observed. The Ni current collector layer and Ni-Zr0.1SDC anode functional layer can be identified and show intimate contact with one another. Further EDS analysis indicates that Ni elements are mainly confined within the Ni-current collector layer and Ni-Zr0.1SDC anode functional layer (Fig. **8b**). Zr elements are mainly located in the substrate and YSZ electrolyte layer (Fig. **8d**). Interestingly, C elements were primarily located in the substrate (Fig. **8c**). Quantitative line EDS analysis (Fig. **8e**) indicates that some carbon elements could still be detected in the Ni current collector layer but not in the Ni-Zr0.1SDC anode functional layer. It is noteworthy that such a Ni current collector region is directly connected to a microchannel in the substrate, whereby methane diffusion to the current collector is relatively easy.

To understand the mechanisms and reactions in the anode and the prevention of carbon deposition in the anode functional layer, the experimental data mentioned above is further compared and interpreted from a theoretical point of view. When methane is employed as fuel for Ni-cermet anode, very complicated

chemical/electrochemical reactions would take place. These could include the steam reforming reaction of CH_4, the dry (CO_2) reforming reaction of CH_4, and water gas shift reaction, as shown below, respectively,

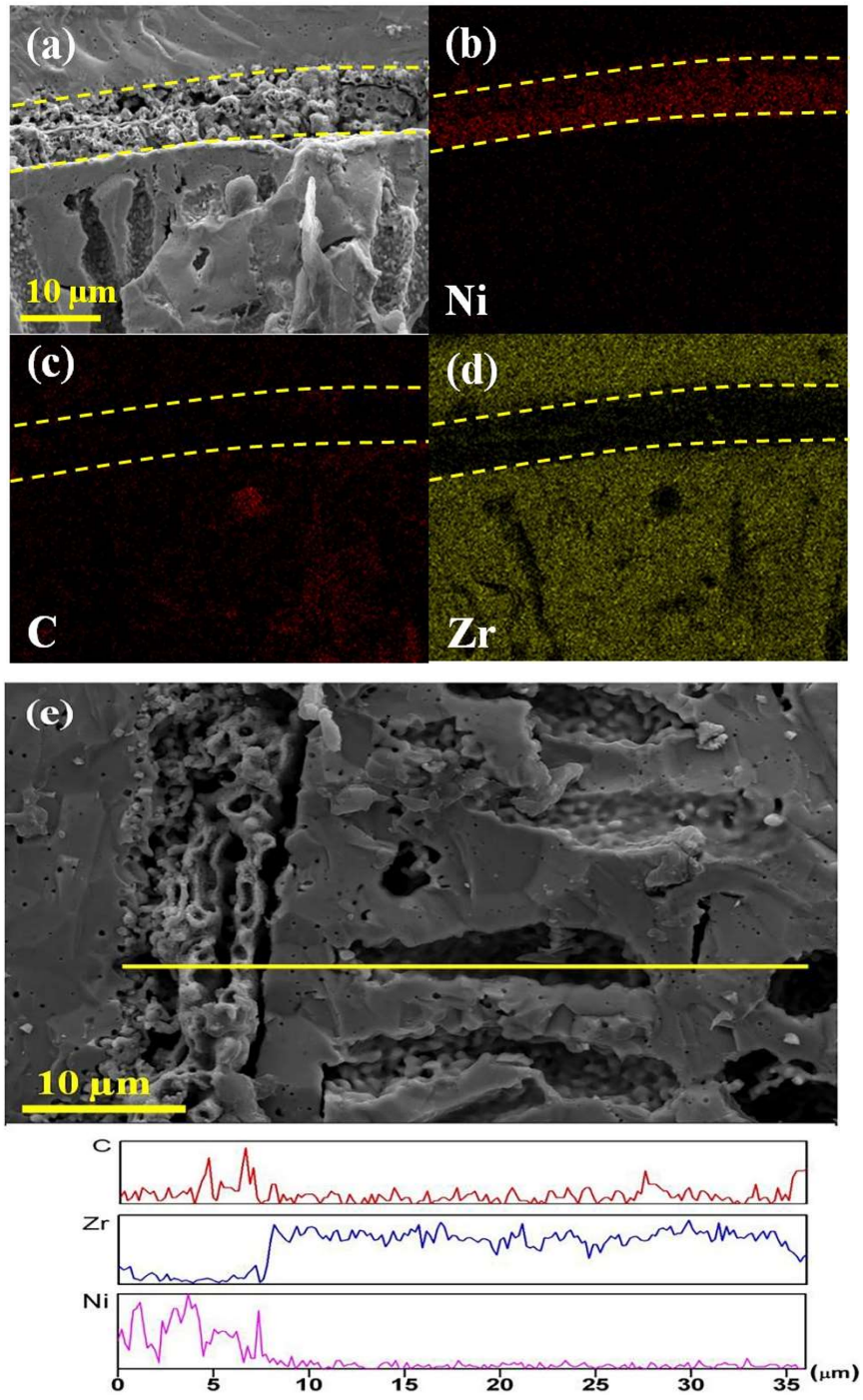

Figure 8: SEM and EDS images of the single cell after stability measurement. (a) Cross sectional SEM image of the single cell. (b) EDS mapping of Ni. (c) EDS mapping of C. (d) EDS mapping of Zr. (e) Location for line EDS characterization and C, Zr, Ni line EDS spectrum.

Steam reforming reaction: $CH_4 + H_2O \leftrightarrow CO + 3H_2$ (1)

Dry reforming reaction: $CH_4 + CO_2 \leftrightarrow 2CO + 2H_2$ (2)

Water-gas shift reaction: $CO + H_2O \leftrightarrow CO_2 + H_2$ (3)

As a result, the fuel species of H_2 and CO are generated from these three reactions, meanwhile CO_2 is produced from the water gas shift reaction. Electrochemical oxidations of fuel species CH_4, H_2, and CO would then take place at triple phase boundaries (TPBs) in the anode functional layer by using oxygen ions released from the Zr0.1SDC phase. Depending on the amount of CH_4 and oxygen ion (O^{2-}) available at TPB sites, both full and partial electrochemical oxidations could occur, specifically,

Full oxidation of CH_4: $\mathrm{CH_4 + 4O^{2-} \rightarrow CO_2 + 2H_2O + 8e^-}$ (4)

Partial oxidation of CH_4: $\mathrm{CH_4 + O^{2-} \rightarrow CO + 2H_2 + 2e^-}$ (5)

$$\mathrm{H_2 + O^{2-} \rightarrow H_2O + 2e^-} \quad (6)$$

$$\mathrm{CO + O^{2-} \rightarrow CO_2 + 2e^-} \quad (7)$$

According to the Nernst potential equation, the OCV of the cell is dependent on the partial pressures of oxidant at the cathode side and fuels at the anode side. Since three fuel species of CH_4, H_2, and CO directly involved in electrochemical oxidations through the reactions of (4) – (7), the OCV of the cell would be determined by these four reactions in a combinational way. Theoretically, it has been demonstrated that the OCVs for electrochemical oxidations of H_2 and CO, and the full electrochemical oxidation of CH_4 decrease with increasing operating temperatures while that for partial electrochemical oxidation of CH_4 increases distinctly [39]. As demonstrated above, the OCVs of the cell fueled with H_2 decreased from 1.01 to 0.94 V when the temperature was increased from 600 to 800°C, which is consistent with the theoretical predictions. With CH_4 as fuel, the OCVs of the cell decreased from 1.02 to 0.967 V with increasing the temperature from 600 to 800°C. This observation indicates that the OCVs contributed by the full electrochemical oxidations of CH_4, H_2, and CO outperformed the contribution from the partial electrochemical oxidation of CH_4, and the latter is not a dominant reaction in the anode. As mentioned above, the type of electrochemical oxidations of CH_4 is dependent on the concentrations of gas species CH_4 and oxygen ion (O^{2-}) at TPB sites. According to the reactions (4) and (5), when CH_4 concentration is relatively low while that of mobile O^{2-}near the TPB sites are relatively high, the full oxidation of CH_4 would occur; in other extreme situations of high CH_4 concentration and low concentration of mobile O^{2-}, the partial oxidation of CH_4 could take place. We have experimentally demonstrated that the microtubular substrate with radially well-aligned microchannels facilitates facile gas diffusion and is able to obtain very high gas permeability [35, 36]. Accordingly, sufficiently high CH_4 concentration would be maintained in the anode functional layer. Since the full oxidation of CH_4 in combination with the oxidations of H_2, and CO outperformed the partial oxidation of CH_4 in the anode functional layer, as demonstrated by the OCVs of the cell, it is reasonable to assume that sufficient oxygen ions are available for these reactions at the TPBs in the anode functional layer. This indicates the good oxygen storage capacity and catalytic property of the Zr0.1SDC phase, which is consistent with the above understanding of Zr doped SDC material.

When CH_4 is directly utilized as fuel for SOFCs, carbon could be generated through three reactions, including direct cracking of CH_4, Boudouard reaction, and hydrogenation, in particular,

Direct cracking of CH_4: $CH_4 \leftrightarrow 2H_2 + C$ (8)

Boudouard reaction: $2CO \leftrightarrow CO_2 + C$ (9)

Hydrogenation: $CO + H_2 \leftrightarrow H_2O + C$ (10)

The reaction of CH_4 direct cracking is usually obtained by Ni's excellent catalytic activity. For the studied microtubular cell, the Ni phase is confined within the thin Ni current collector layer and Ni-Zr0.1SDC anode functional layer. Since H_2O and CO_2 are produced only in the thin anode functional layer through electrochemical oxidization of fuels, which facilitates the reforming reactions of CH_4 and water gas shift reaction, it is less likely for direct CH_4 cracking (reaction (8)) to occur in the thin Ni-containing layers. Therefore, carbon could be produced only through the Boudouard reaction (9) and hydrogenation (10). When the concentrations of H_2O and CO_2 are relatively high, which is usually the case in the thin anode functional layer, the backward reactions of (9) and (10) would be favorited. As a result, carbon accumulation would be inhibited in the anode functional layer. This could

be why the cell demonstrated very stable performance in the short-term test when directly fueled with methane. Depending on various species concentrations, the forward Boudouard reaction and hydrogenation could still occur in the YSZ microstructure substrate, and carbon could be built up in the substrate and current collector region near microchannels. This understanding is also consistent with the above EDS results of carbon element distribution.

4. Conclusions

A family of NiO 50%-$Ce_{0.8-x}Sm_{0.2}Zr_xO_{2-\delta}$ 50% in weight (x = 0.0, 0.05, 0.10, 0.15, 0.20) anode composite powders were successfully synthesized using urea combustion method in one pot. The Zr doping effects were systematically studied using symmetric cells in a reducing atmosphere at elevated temperatures. The Zr doping level of x = 0.1 that minimizes the anodic polarization resistance of the composite anode was identified. Microtubular YSZ substrate was fabricated using an in-house built spinning extrusion system, featuring radially well-aligned microchannels open at the substrate inner surface. Built upon the fabrication of thick YSZ substrate, thin layers of NiO current collector, NiO-Zr0.1SDC anode, YSZ/SDC electrolyte, and LSCF cathode were sequentially fabricated through dip-coating/sintering process alternatively, forming a microtubular cell of YSZ substrate/NiO/NiO-Zr0.1SDC/YSZ/SDC/LSCF. The cell exhibited the peak power densities of 602 and 456 mW cm^{-2} at 800℃ when ambient air was used as an oxidant, and humidified hydrogen and methane were used as fuel, respectively. The cell also exhibited very good performance stability in the 26 hrs short-term durability test at 700°C near the condition of peak power density output when directly fueled with methane. The capability of carbon deposition prevention was achieved through a synergistic combination of oxygen storage and catalytic properties of the Zr0.1SDC phase in the anode functional layer and novel architecture design of the cell. The fundamental mechanisms for carbon suppression are analyzed.

References

[1] Ormerod RM. Chem Soc Rev. 2003; 32: 17. https://doi.org/10.1177/1030570X0301600102

[2] Minh N. Solid State Ionics, 2004; 174: 271. https://doi.org/10.1016/j.ssi.2004.07.042

[3] Zhan Z, Barnett SA. Science, 2005; 308: 844. https://doi.org/10.1126/science.1109213

[4] Nakagawa N. Ishida M. Ind Eng Chem Res. 1988; 27: 1181. https://doi.org/10.1021/ie00079a016

[5] Yang L, Wang S, Blinn K, Liu M, Liu Z, Cheng Z, Liu M. Science 2009; 326: 126. https://doi.org/10.1126/science.1174811

[6] Takeguchi T, Kikuchi R, Yano T, Eguchi K, Murata K. Catal Today 2003; 84: 217. https://doi.org/10.1016/S0920-5861(03)00278-5

[7] Sumi H, Yamaguchi T, Hamamoto K, Suzuki T, Fujishiro Y. J Power Sources 2012; 220: 74. https://doi.org/10.1016/j.jpowsour.2012.07.106

[8] Kim Y, Kim JH, Bae J, Yoon CW, Nam SW. J. Phys Chem C 2012; 116: 13281. https://doi.org/10.1021/jp3035693

[9] Miao H, Liu G, Chen T, He C, Peng J, Ye S, Wang WG. J Solid State Electrochem. 2015; 19: 639. https://doi.org/10.1007/s10008-014-2640-7

[10] Myung J, Kim SD, Shin TH, Lee D, Irvine JTS, Moon J, Hyun SH. J Mater Chem A 2015; 3: 13801. https://doi.org/10.1039/C4TA06037G

[11] Zhu H, Wang W, Ran R, Shao Z. Int J Hydrog Energy, 2013; 38: 3741. https://doi.org/10.1016/j.ijhydene.2013.01.032

[12] Suzuki T, Yamaguchi T, Hamamoto K, Fujishiro Y, Awano M, Sammes N. Energy Environ Sci. 2011; 4: 940. https://doi.org/10.1039/C0EE00231C

[13] Wang K, Ran R, Shao Z. J Power Sources 2007; 170: 251. https://doi.org/10.1016/j.jpowsour.2007.03.070

[14] Yoon D, Manthiram A. Energy Environ Sci. 2014, 7, 3069. https://doi.org/10.1039/C4EE01455C

[15] Ma J, Jiang C, Connor PA, Cassidy M, Irvine JTS. J Mater Chem A 2015; 3: 19068. https://doi.org/10.1039/C5TA06421J

[16] Kim H, Lu C, Worrell WL, Vohs JM, Gorte RJ. J Electrochem Soc. 2002; 149: A247. https://doi.org/10.1149/1.1445170

[17] Nikolla E, Schwank J, Linic S. J Electrochem Soc. 2009; 156: B1312. https://doi.org/10.1149/1.3208060

[18] Wu X, Zhou X, Tian Y, Kong X, Zhang J, Zuo W. Int J Hydrog Energy 2015; 40: 16484. https://doi.org/10.1016/j.ijhydene.2015.09.121

[19] Qiao J, Zhang N, Wang Z, Mao Y, Sun K, Yuan Y. Fuel Cells, 2009; 9: 729. https://doi.org/10.1002/fuce.200800104

[20] Tao S, Irvine JTS. Nat Mater, 2003; 2: 320. https://doi.org/10.1038/nmat871

[21] Atkinson A, Barnett S, Gorte RJ, Irvine JTS, McEvoy AJ, Mogensen M, *et al*. Nat Mater. 2004; 3: 17. https://doi.org/10.1038/nmat1040

[22] Huang YH, Dass RI, Xing ZL, Goodenough JB. Science 2006; 312: 254. https://doi.org/10.1126/science.1125877

[23] Sengodan S, Choi S, Jun A, Shin TH, Ju YW, Jeong HY, *et al*. Nat Mater. 2015; 14: 205. https://doi.org/10.1038/nmat4166

[24] Dong G, Yang C, He F, Jiang Y, Ren C, Gan Y, *et al*. RSC Adv. 2017; 7: 22649. https://doi.org/10.1039/C7RA03143B

[25] Wang W, Su C, Wu Y, Ran R, Shao Z. Chem Rev. 2013; 113: 8104. https://doi.org/10.1021/cr300491e

[26] McIntosh S, Gorte RJ. Chem Rev. 2004; 104: 4845. https://doi.org/10.1021/cr020725g

[27] Lin Y, Zhan Z, Barnett SA., J Power Sources 2006; 158: 1313. https://doi.org/10.1016/j.jpowsour.2005.09.060

[28] Zhu H, Colclasure AM, Kee RJ, Lin Y, Barnett SA. J Power Sources 2006; 161: 413. https://doi.org/10.1016/j.jpowsour.2006.04.101

[29] Bierschenk DM, Pillai MR, Lin Y, Barnett SA. Fuel Cells, 2010; 10: 1129. https://doi.org/10.1002/fuce.201000005

[30] Novik NN, Konakov VG, Archakov IY. Rev Adv Materi Sci. 2015; 40: 188.

[31] Zhao K, Du Y. J Power Sources 2017; 347: 79. https://doi.org/10.1016/j.jpowsour.2017.01.113

[32] Larrondo S, Vidal M, Irigoyen B, Craievich AF, Lamas DG, Fabregas IO, *et al*. Catal Today, 2005; 107: 53. https://doi.org/10.1016/j.cattod.2005.07.110

[33] Laguna OH, Sarria FR, Centeno MA, Odriozola JA. J Catalysis 2010; 276: 360. https://doi.org/10.1016/j.jcat.2010.09.027

[34] Venkataramana K, Madhusudan C, Madhuri C, Reddy CV. Materials Today: Proceedings 3, 2016; 3: 3908. https://doi.org/10.1016/j.matpr.2016.11.048

[35] Ren C, Gan Y, Lee M, Yang C, He F, Jiang Y. *et al*. J Electrochem Soc. 2016; 163: F1115 https://doi.org/10.1149/2.1271609jes

[36] Ren C, Gan Y, Yang C, Lee M, Dong G, Xue X. J Electrochem Soc. 2017; 164: F722. https://doi.org/10.1149/2.0311707jes

[37] Ren C, Gan Y, Yang C, Lee M, Green RD, Xue X. J Appl Electrochem. 2018; 48: 959. https://doi.org/10.1007/s10800-018-1225-z

[38] Lee MJ, Jung JH, Zhao K, Kim BH, Xu Q, Ahn BG, *et al*. J Eur Ceram Soc. 2014; 34: 1771. https://doi.org/10.1016/j.jeurceramsoc.2013.12.042

[39] Panthi D, Choi B, Tsutsumi A. J Solid State Electrochem. 2017; 21: 255. https://doi.org/10.1007/s10008-016-3366-5